



Article

Loop2 Size Modification Reveals Significant Impacts on the Potency of α -Conotoxin TxID

Jianying Dong¹, Panpan Zhang¹, Junjie Xie¹, Ting Xie¹, Xiaopeng Zhu¹ , Dongting Zhangsun², Jinpeng Yu^{1,*} and Sulan Luo^{1,2,*} 

¹ School of Medicine, Guangxi University, Nanning 530004, China; 2028301003@st.gxu.edu.cn (J.D.)

² Key Laboratory of Tropical Biological Resources, Ministry of Education, Key Laboratory for Marine Drugs of Haikou, Hainan University, Haikou 570228, China

* Correspondence: yujinpeng@gxu.edu.cn (J.Y.); sulan2021@gxu.edu.cn (S.L.)

Abstract: α 4/6-conotoxin TxID, which was identified from *Conus textile*, simultaneously blocks rat (*r*) α 3 β 4 and α 6/ α 3 β 4 nicotinic acetylcholine receptors (nAChRs) with IC₅₀ values of 3.6 nM and 33.9 nM, respectively. In order to identify the effects of loop2 size on the potency of TxID, alanine (Ala) insertion and truncation mutants were designed and synthesized in this study. An electrophysiological assay was used to evaluate the activity of TxID and its loop2-modified mutants. The results showed that the inhibition of 4/7-subfamily mutants [+9A]TxID, [+10A]TxID, [+14A]TxID, and all the 4/5-subfamily mutants against α 3 β 4 and α 6/ α 3 β 4 nAChRs decreased. Overall, ala-insertion or truncation of the 9th, 10th, and 11th amino acid results in a loss of inhibition and the truncation of loop2 has more obvious impacts on its functions. Our findings have strengthened the understanding of α -conotoxin, provided guidance for further modifications, and offered a perspective for future studies on the molecular mechanism of the interaction between α -conotoxins and nAChRs.

Keywords: α -conotoxin TxID; α 3 β 4 nAChR; loop size modification; electrophysiology; CD spectra



Citation: Dong, J.; Zhang, P.; Xie, J.; Xie, T.; Zhu, X.; Zhangsun, D.; Yu, J.; Luo, S. Loop2 Size Modification Reveals Significant Impacts on the Potency of α -Conotoxin TxID. *Mar. Drugs* **2023**, *21*, 286. <https://doi.org/10.3390/md21050286>

Academic Editors: Alessia Belgi and Andrea Jane Robinson

Received: 5 April 2023

Revised: 27 April 2023

Accepted: 29 April 2023

Published: 1 May 2023



Copyright: © 2023 by the authors. Licensee MDPI, Basel, Switzerland. This article is an open access article distributed under the terms and conditions of the Creative Commons Attribution (CC BY) license (<https://creativecommons.org/licenses/by/4.0/>).

1. Introduction

Nicotinic acetylcholine receptors (nAChRs) are pentameric ligand-gated ion channels that surround a central water pore [1,2]. They are classified into neuronal nAChRs and muscle-type nAChRs based on their wide distribution in the central and peripheral nervous systems, as well as in non-nervous tissues. Previous studies have shown that nAChRs have 17 distinct subunits: α 1– α 10, β 1– β 4, δ , ϵ , and γ . The α 1, β 1, δ , ϵ , and γ subunits form muscle-type nAChRs, whereas the γ subunit is only present in mammalian embryonic cells. The remaining α and β subunits combine to form neuronal nAChR subtypes, including homo-pentamers composed of only α subunits (such as α 7 and α 9 α 10 nAChRs) and hetero-pentamers composed of α and β subunits in different ratios (α 3 β 4, α 4 β 2, α 6 β 4 nAChRs, etc.). Each nAChR subunit comprises a certain proportion of various nAChR subtypes with different pharmacological properties [3–5].

The results of polymerase chain reaction experiments have shown significant RNA expression of α 3 and β 4 subunits in the human adrenal medulla, human adrenal chromophores, and human cervical squamous carcinoma cells (SiHa) [6,7]. α 3 β 4 nAChR is also significantly expressed in regions of the brain, such as the habenular-internuclear pathway, the hippocampus, the hypothalamus, and the pineal gland [8–10]. It is a key regulator of reward-related behaviors in the habenular-internuclear pathway, and is also involved in nicotine-mediated appetite loss in the hypothalamus [11–13]. α 6-containing (α 6*) nAChRs are expressed throughout the peripheral and central nervous systems [14–16]. α 6 β 4 nAChR is concentrated in rat dorsal medullary ganglion neurons, which are associated with chronic pain and have become an expected therapeutic target [17,18]. Overall, the distributions of α 3 β 4 and α 6 β 4 nAChRs overlap in some tissues, and the extra-cellular domains (ECDs) of

the two receptors are highly homologous. This study will further explain the mechanism of α -conotoxins binding to $\alpha 3\beta 4$ and $\alpha 6\beta 4$ nAChRs and will facilitate the modification and development of targeted drugs.

The cone snails (*Conus*) are a large family of preying gastropods that is currently known to have more than 700 species. Each species of cone snail can secrete 50–200 different kinds of small molecule polypeptides, called conotoxins, in their venom duct, which possess rich pharmacological activities [19,20]. With the improved accuracy of detection technology, it is conservatively estimated that there are over hundreds of thousands of distinct neuroactive conopeptides [21,22]. Among the abundant conotoxins, α -conotoxins from the A-superfamily are the largest subfamily. They are selective and potent antagonists of nAChRs and could be used to distinguish between different nAChR subtypes [23–25]. α -conotoxins are usually composed of 12 to 20 amino acids and four cysteines (Cys) arranged in the form of “CC–C–C”, which forms a “globular” pattern (Cys I—III and Cys II–IV). Two pairs of disulfide bonds are found in most native α -conotoxins [26,27]. Based on the number of amino acid residues in the two Cys loops, α -conotoxins can be further classified into 3/5, 4/3, 4/4, 4/5, 4/6, and 4/7 subfamilies [19,28].

TxID, an $\alpha 4/6$ -conotoxin identified from *Conus textile*, is a competitive antagonist inhibitor with a potent blockade effect on $\alpha 3\beta 4$ nAChRs, with an IC_{50} value of 3.6 nM. However, TxID also inhibits the $\alpha 6/\alpha 3\beta 4$ nAChR, with an IC_{50} of 33.9 nM [29]. In previous studies, TxID was found to inhibit the growth of human non-small-cell lung cancer A549 and NCI-H1299 cell lines, while displaying an enhanced inhibitory effect when simultaneously treated with adriamycin [30]. TxID was shown to significantly inhibit the proliferation of SiHa [6].

The first Cys loop (loop1) of α -conotoxin contains three amino acids that mainly target muscle-type nAChRs, such as GI, MI, SI, SIA, and SII, whereas $\alpha 4/7$ -conotoxins are specific inhibitors of neuronal nAChRs [31–33]. The number of amino acids contained in loop2 of α -conotoxins also affects their functions. For example, $\alpha 4/6$ -conotoxins AuIB, TxID, and VnIB showed higher selectivity for $\beta 4^*$ nAChRs than $\beta 2^*$ nAChRs, whereas $\alpha 4/7$ -conotoxins MII, OmIA, PIA, TxIB, RegIIA, and PeIA showed higher selectivity for $\beta 2^*$ nAChRs [34–38]. Previous findings have shown that a mutation of asparagine (Asn, N) to leucine (Leu, L) at the twelfth position of LsIA enhanced the activity of $\alpha 3\beta 4$ nAChRs [39]. Compared with wild-type RegIIA, [N11A, N12A]RegIIA showed almost a complete loss of potency against human (h) $\alpha 7$, $\alpha 3\beta 2$, and $\alpha 6/\alpha 3\beta 4\beta 3$ nAChRs, whereas the potency against $\alpha 3\beta 4$ nAChRs was only decreased 10-fold; thus, [N11A, N12A]RegIIA selectively inhibited $\alpha 3\beta 4$ nAChRs [40]. Studies of [A10L]PnIA have shown that truncation of the twelfth to fifteenth amino acid residues in loop2 causes [A10L]PnIA to lose its activity against $\alpha 7$ nAChRs [41].

In this study, the amino acids of TxID loop2 were truncated and inserted into alanine (Ala, A), and the activity of TxID mutants was detected using electrophysiology. This will enrich studies on the function of loop2 for α -conotoxins and will also provide a basis for further understandings of the binding mechanism between $\alpha 4/6$ -conotoxin TxID and $\alpha 3\beta 4$ nAChRs.

2. Results

2.1. Synthesis and Characterization of TxID and Its Mutants

Because the “globular” isomer is the natural and bioactive form of the native TxID, a two-step oxidative folding protocol was used for the oxidation of TxID and all the loop2 size mutants with this disulfide bond arrangement (Figure 1). Afterward, the purity and identity were confirmed by analytical reversed-phase high-performance liquid chromatography (RP-HPLC) and electrospray ionization mass spectroscopy (ESI-MS) (Figures S1 and S2, Table 1).

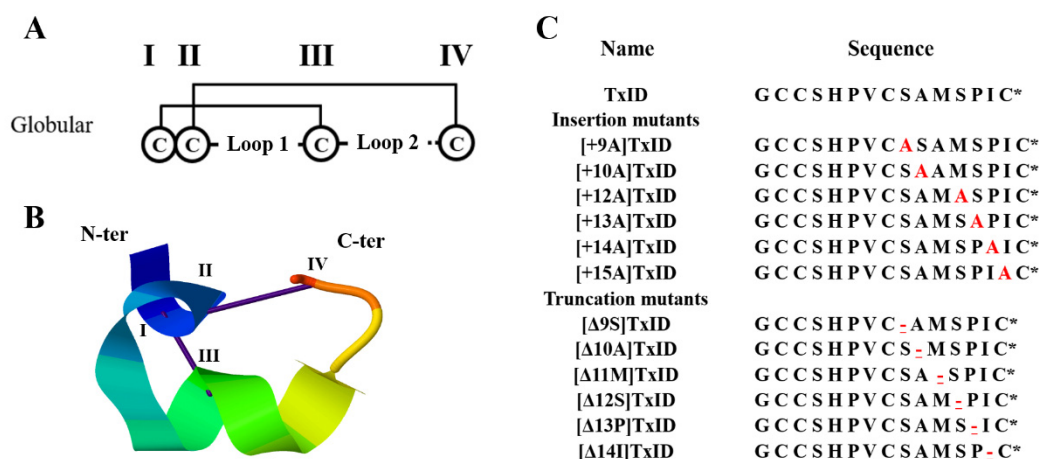


Figure 1. Disulfide bond arrangement and sequences of TxID and its mutations. The disulfide bond arrangement of α -conotoxins is CysI-CysIII and CysII-CysIV, which form two cysteine loops (loop1 and loop2). TxID and its mutants are all globular isomers; “I–IV” indicate the four cysteines in the sequence (A). Structure of the globular TxID (PDB: 2m3i); the N- and C-termini are labeled with N-ter and C-ter, respectively (B). The inserted alanine is marked red; “-” indicates the truncated amino acid site, which is underlined and marked in red; “*” indicates the C-terminal amide (C).

Table 1. ESI-MS identified the molecular weight of TxID and its mutants.

Peptides	Retention Time (min)	Elution Concentration of Solvent B ^a (%)	Theoretical MW (Da)	Experimental MW (Da)
TxID	15.08	27.6	1489.79	1489.16
Insertion mutants				
[+9A]TxID	20.10	35.2	1560.87	1560.78
[+10A]TxID	16.68	30.0	1560.87	1560.64
[+12A]TxID	16.72	30.1	1560.87	1560.50
[+13A]TxID	15.79	28.7	1560.87	1560.38
[+14A]TxID	17.00	30.5	1560.87	1560.78
[+15A]TxID	17.19	30.8	1560.87	1560.9
Truncation mutants				
[Δ9S]TxID	15.46	28.2	1402.72	1402.12
[Δ10A]TxID	20.82	36.2	1418.72	1418.62
[Δ11M]TxID	17.75	31.6	1358.60	1358.56
[Δ12S]TxID	16.78	30.2	1402.72	1402.52
[Δ13P]TxID	18.12	32.2	1392.68	1392.22
[Δ14I]TxID	15.57	28.4	1376.64	1376.66

^a Solvent B is 90% ACN and 10% ddH₂O with 0.05% TFA.

2.2. Circular Dichroism of TxID and Its Mutants

The circular dichroism (CD) spectra were utilized to analyze whether the loop2 modification had any effect on the secondary structure of TxID. The results indicated that the wild-type (WT) TxID and its mutants showed negative peaks at 208 nm and 222 nm, indicating that all the peptides contain α -helices (Figure 2, Table 2). The percentage of secondary structures were almost identical between the WT-TxID and mutants, with the truncated mutant [Δ13P]TxID showing the largest change. The proportion of α -helices in [Δ13P]TxID decreased by ten percent compared to the native TxID, whereas the proportion of β -sheets increased by twelve percent.

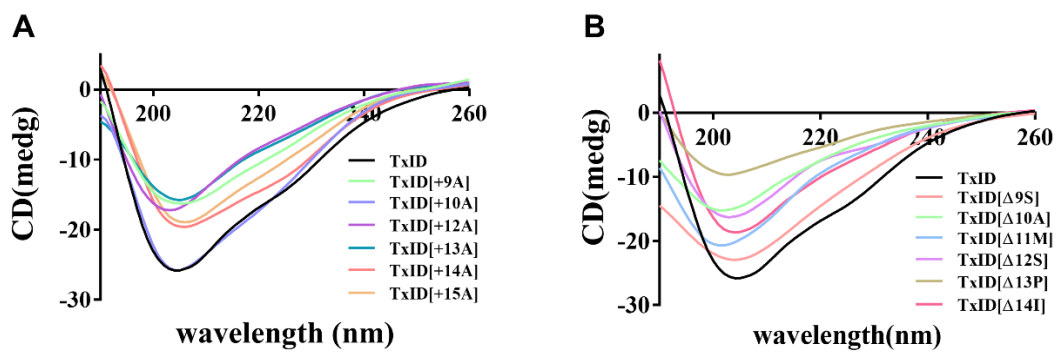


Figure 2. CD spectra of TxID and its insertion (A) and truncation mutants (B) in H₂O, *n* = 3. All the peptides have negative peaks at 208 nm and 222 nm, whereas the shapes of the peaks are similar, so the secondary structures of wild-type TxID and its mutants are almost identical.

Table 2. Secondary structure percentages of the native TxID and its mutants.

Peptides	α -Helix (%)	β -Sheet (%)	β -Turn (%)	Random Coil (%)
TxID	19%	21%	27%	33%
[+9A]TxID	14%	26%	25%	35%
[+10A]TxID	20%	23%	27%	29%
[+12A]TxID	12%	28%	24%	36%
[+13A]TxID	15%	25%	25%	35%
[+14A]TxID	19%	20%	25%	35%
[+15A]TxID	17%	24%	26%	33%
[Δ 9S]TxID	14%	32%	26%	28%
[Δ 10A]TxID	11%	30%	25%	34%
[Δ 11M]TxID	14%	27%	26%	34%
[Δ 12S]TxID	13%	27%	26%	34%
[Δ 13P]TxID	9%	33%	24%	33%
[Δ 14I]TxID	12%	29%	24%	34%

2.3. Inhibition of TxID and Its Mutants on $\alpha 3\beta 4$ and $\alpha 6/\alpha 3\beta 4$ nAChRs

The potency of TxID and its mutants on the $\alpha 3\beta 4$ and $\alpha 6/\alpha 3\beta 4$ nAChR subtypes was evaluated by electrophysiology. The results showed that the IC₅₀ values of TxID inhibiting $\alpha 3\beta 4$ and $\alpha 6/\alpha 3\beta 4$ nAChRs were 5.3 nM and 33 nM, respectively (Figures 3, 4A and 5A, Table 3).

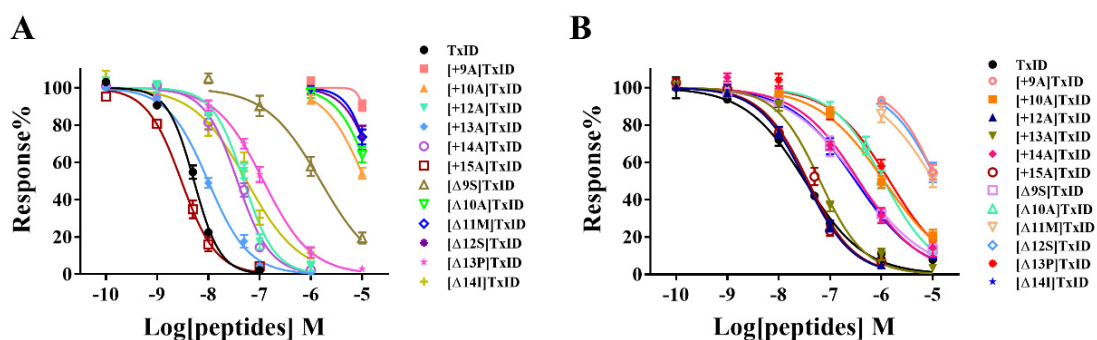


Figure 3. Dose–response curves of wild-type TxID and its mutants on $\alpha 3\beta 4$ (A) and $\alpha 6/\alpha 3\beta 4$ nAChRs (B). The dose–response curves of most TxID mutants are right-shifted compared to wild-type TxID, whereas only the curve of [+15A]TxID interacting with $\alpha 3\beta 4$ nAChRs is slightly left-shifted. Each data point represents the mean \pm SEM values from at least 4–10 oocytes.

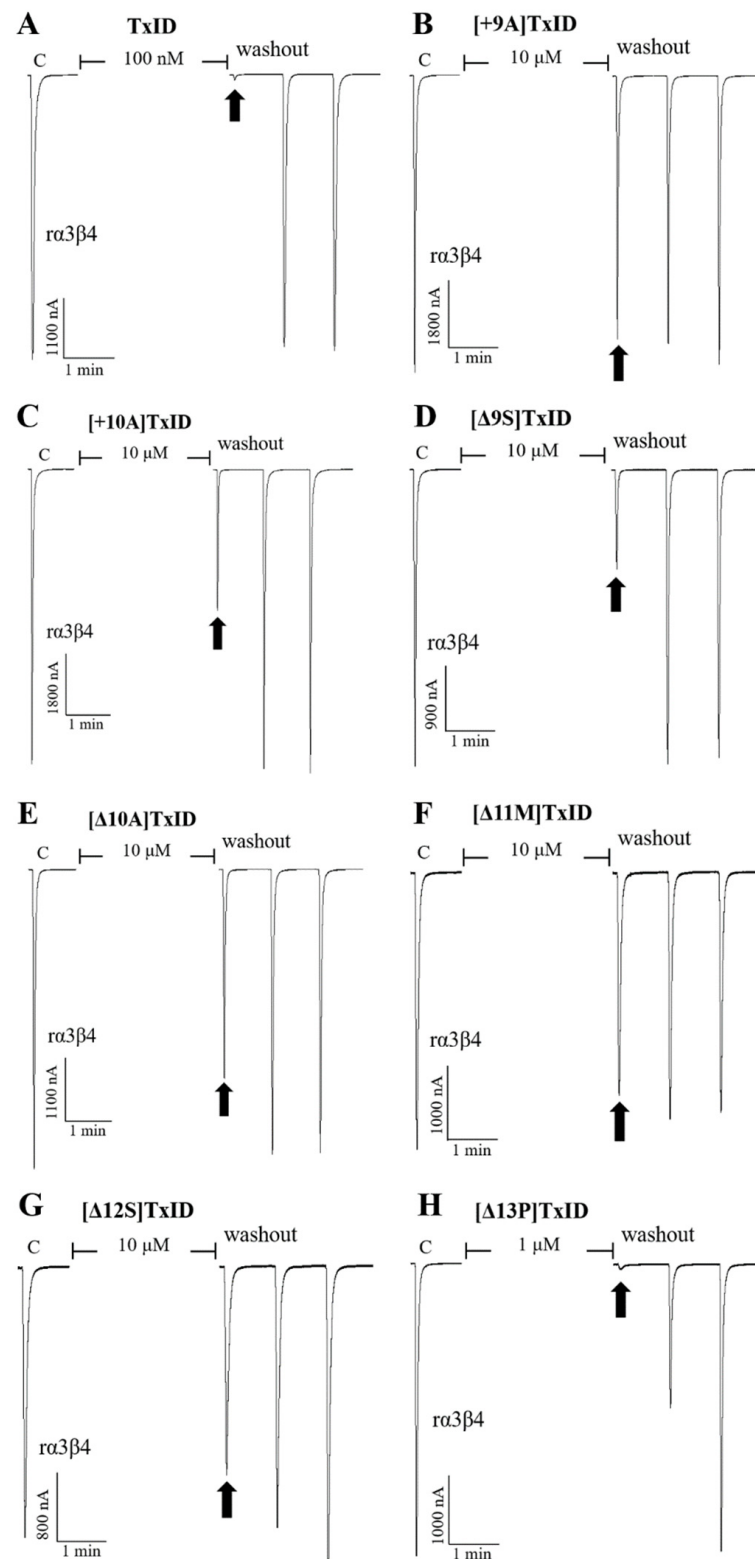


Figure 4. Blocking effects of TxiD (A) and part of the mutants (B–H) on $\alpha 3\beta 4$ nAChRs. Representative responses in individual oocytes are revealed. The arrows indicate the currents generated by 100 μM of ACh stimulation after incubation with different concentrations of α -conotoxins for 5 min. “C” indicates the response to 100 μM of ACh as a control.

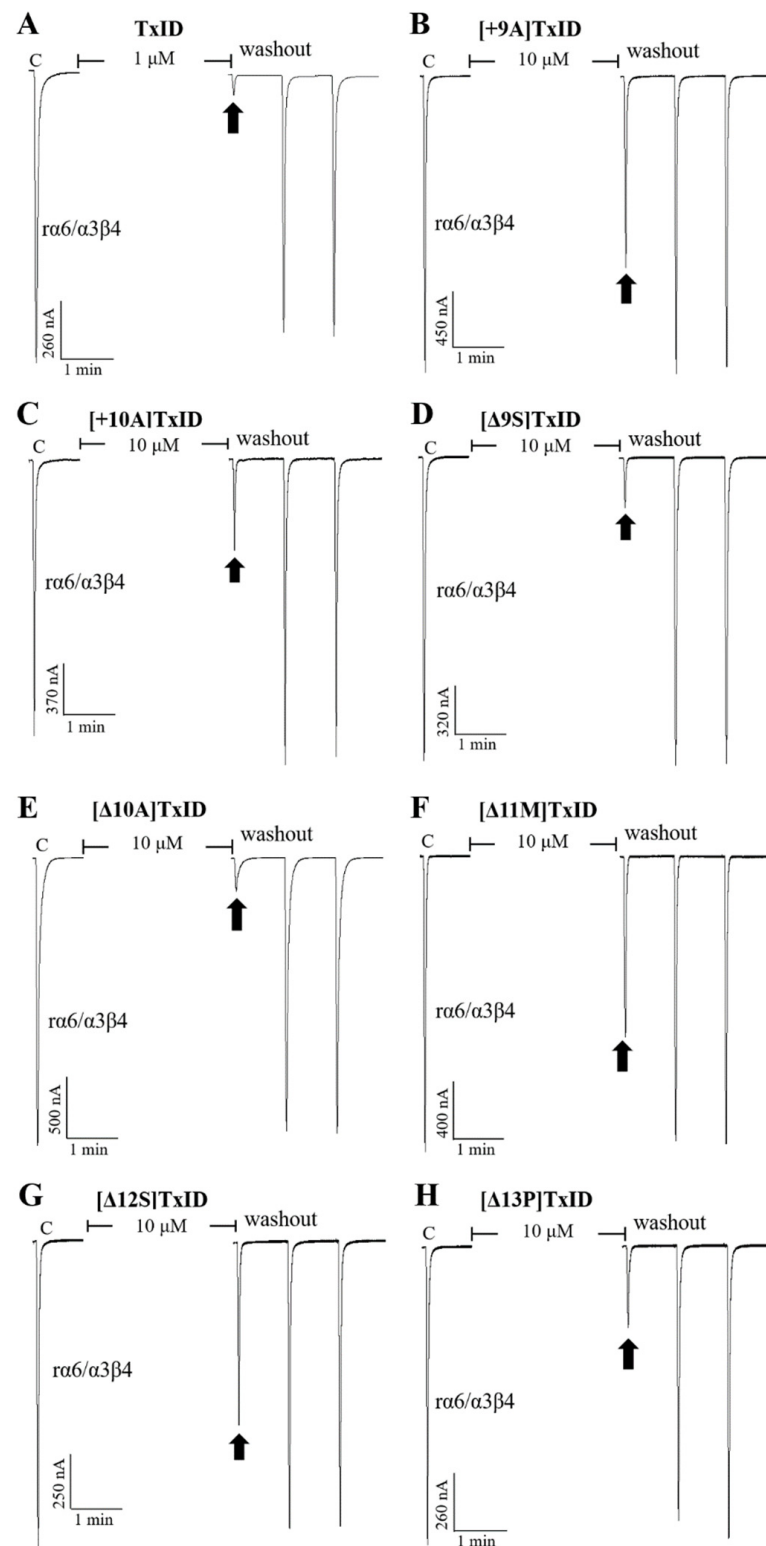


Figure 5. Blocking effects of TxID (A) and part of the mutants (B–H) on $r\alpha 6/\alpha 3\beta 4$ nAChRs. Representative responses in individual oocytes are revealed. The arrows indicate the currents generated by 100 μM of ACh stimulation after incubation with different concentrations of α -conotoxins for 5 min. “C” indicates the response to 100 μM of ACh as a control.

Table 3. The potency and selectivity of the native TxID and its mutants against $\alpha 3\beta 4$ and $\alpha 6/\alpha 3\beta 4$ nAChRs.

WT and Mutant Peptides	$\alpha 3\beta 4$		Ratio Relative to TxID ^b	$\alpha 6/\alpha 3\beta 4$		Ratio Relative to TxID ^b
	IC ₅₀ (95% CI) ^a (nM)	Hill Slope		IC ₅₀ (95% CI) ^a (nM)	Hill Slope	
TxID	5.3 (4.8–5.7)	1.7 (1.4–2.1)	1.0	33 (28–38)	0.8 (0.7–0.9)	1.0
Insertion mutants						
[+9A]TxID	>10,000 ^c	/	/	>10,000 ^c	/	/
[+10A]TxID	>10,000 ^c	/	/	1130 (873–1480)	0.7 (0.6–0.8)	34
[+12A]TxID	49 (42–57)	1.4 (1.1–2.2)	9.2	34 (28–40)	1.0 (0.8–1.1)	1.0
[+13A]TxID	9.9 (8.6–11)	1.1 (1.0–1.3)	1.9	64 (53–77)	1.0 (0.8–1.2)	2.0
[+14A]TxID	37 (32–42)	1.3 (1.1–1.6)	7.0	368 (271–504)	0.7 (0.6–0.9)	11
[+15A]TxID	3.0 (2.6–3.5)	1.3 (1.1–1.6)	0.6	37 (31–45)	1.0 (0.8–1.1)	1.1
Truncation mutants						
[Δ9S]TxID	1546 (1079–2275)	0.8 (0.6–1.1)	292	351 (271–458)	0.6 (0.5–0.7)	11
[Δ10A]TxID	>10,000 ^c	/	/	1120 (899–1437)	0.9 (0.7–1.1)	34
[Δ11M]TxID	>10,000 ^c	/	/	>10,000 ^c	/	/
[Δ12S]TxID	>10,000 ^c	/	/	>10,000 ^c	/	/
[Δ13P]TxID	119 (99–146)	0.9 (0.8–1.1)	22	1448 (1092–1911)	0.8 (0.6–0.9)	44
[Δ14I]TxID	56 (44–72)	0.8 (0.7–1.1)	11	316 (243–410)	0.7 (0.6–0.8)	9.6

^a IC₅₀ values are reported with 95% confidence intervals. ^b Ratio of mutant TxID to wild-type TxID IC₅₀ values. ^c The current responses induced by 100 μM of acetylcholine (ACh) are >50% after incubation with 10 μM of peptides.

10 μM [+9A]TxID and [+10A]TxID did not completely inhibit $\alpha 3\beta 4$ nAChRs, and the blocking percentages were less than fifty percent (Figures 3 and 4B,C, Table 3). The potency of [+12A]TxID and [+14A]TxID against $\alpha 3\beta 4$ nAChRs decreased 9.2-fold and 7.0-fold, respectively, which are lower potencies compared to that of the native TxID (Figure 3A, Table 3). [+13A]TxID and [+15A]TxID showed similar inhibitory effects of $\alpha 3\beta 4$ nAChRs, with IC₅₀ values of 9.9 nM and 3.0 nM, respectively, which were 1.9-fold and 0.6-fold that of the WT-TxID, respectively (Figure 3A, Table 3).

The activity assays of loop2 truncation mutants also showed that the 4/5-subfamily mutants [Δ10A]TxID, [Δ11M]TxID, and [Δ12S]TxID exhibited a complete loss of activity against $\alpha 3\beta 4$ nAChRs (IC₅₀ > 10 μM), whereas [Δ9S]TxID exhibited a 292-fold decrease in potency, with an IC₅₀ of 1,546 nM (Figures 3A and 4E–G, Table 3). When the truncation sites were closer to the end of the amino acid sequence of TxID, [Δ13P]TxID and [Δ14I]TxID showed a much smaller decrease in activity compared to the other truncation mutants, which showed a 22-fold and 11-fold decrease, with IC₅₀ values of 119 nM and 56 nM, respectively (Figures 3A and 4H, Table 3).

The activity of the insertion mutants was also evaluated on $\alpha 6/\alpha 3\beta 4$ nAChRs. The results demonstrated that [+9A]TxID was the only 4/7-subfamily mutant that displayed no obvious inhibition against $\alpha 6/\alpha 3\beta 4$ nAChRs (Figures 3B and 5B, Table 3). The potency of [+10A]TxID and [+14A]TxID decreased 34-fold and 11-fold, respectively, with IC₅₀ values of 1130 nM and 368 nM, respectively (Figures 3B and 5C, Table 3). The mutants [+12A]TxID, [+13A]TxID, and [+15A]TxID showed similar activity to that of the WT-TxID (Figure 3B, Table 3).

When the potencies of the truncation mutants against $\alpha 6/\alpha 3\beta 4$ nAChRs were assessed, [Δ11M]TxID and [Δ12S]TxID showed no significant blocking effect on $\alpha 6/\alpha 3\beta 4$ nAChRs (Figures 3B and 5F–G, Table 3). Other truncation mutants, including [Δ9S]TxID, [Δ10A]TxID, [Δ13P]TxID, and [Δ14I]TxID, displayed different extents of potency decreases that were relative to the native TxID, with IC₅₀ values of 351 nM, 1120 nM, 1448 nM, and 316 nM, respectively (Figures 3B and 5D,E,H, Table 3).

3. Discussion

The $\alpha 3\beta 4$ and $\alpha 6\beta 4$ nAChRs are all expressed in both the central and peripheral nervous systems. Hence, they are relevant to many diseases and have become popular targets for drug therapy. However, the ECD of $\alpha 6\beta 4$ nAChRs is highly homologous to

that of $\alpha 3\beta 4$ nAChRs, whereas the distribution of these two receptors can overlap in some tissues. Thus, most of the natural α -conotoxins identified to date that selectively target $\alpha 3\beta 4$ nAChRs may also inhibit $\alpha 6\beta 4$ nAChRs, which almost all belong to the 4/7-subfamily and only a few belong to the 4/6-subfamily, including TxID, AuIB, and VnIB (Table 4).

Table 4. Native α -conotoxins that target the $\alpha 3\beta 4$ and $\alpha 6\beta 4$ nAChRs.

Name	Conus	Subfamily	Sequence	IC ₅₀ on $\alpha 3\beta 4$ nAChR (nM)	Selectivity on nAChRs	Ref.
TxID	<i>C. textile</i>	4/6	GCCSHPVCSAMSPIC*	3.6	$\alpha 3\beta 4 > \alpha 6 / \alpha 3\beta 4 > \alpha 2\beta 4$	[29]
AuIB	<i>C. aulicus</i>	4/6	GCCSYPPCFATNPDC*	750	$\alpha 3\beta 4$	[42]
VnIB	<i>C. ventricosus</i>	4/6	GGCCSHPVICYTKPNPCG*	360	$\alpha 6 / \alpha 3\beta 4 > \alpha 3\beta 4 > \alpha 6 / \alpha 3\beta 2\beta 3$	[43]
BuIA	<i>C. bullatus</i>	4/4	GCCSTPPCAVLYC*	27.7	$\alpha 6 / \alpha 3\beta 2\beta 3 > \alpha 6 / \alpha 3\beta 4 > \alpha 3\beta 2 > \alpha 3\beta 4 > \alpha 4\beta 4 > \alpha 7 > \alpha 2\beta 2 = \alpha 2\beta 4$	[44,45]
LvIA	<i>C. lividus</i>	4/7	GCCSHPACNVDHPEIC*	148	$\alpha 3\beta 2 > \alpha 6 / \alpha 3\beta 2\beta 3 > \alpha 6 / \alpha 3\beta 4 > \alpha 3\beta 4 > \alpha 7$	[46]
PeIA	<i>C. pergrandis</i>	4/7	GCCSHPACSVNHPELC*	480	$\alpha 9\alpha 10 > \alpha 6 / \alpha 3\beta 2\beta 3 > \alpha 3\beta 2 > \alpha 6 / \alpha 3\beta 4 > \alpha 3\beta 4 > \alpha 7$	[38,47]
PIA	<i>C. purpurascens</i>	4/7	RDPCCSNPVCTVHNPQIC*	518	$\alpha 6 / \alpha 3\beta 2\beta 3 > \alpha 6 / \alpha 3\beta 4 > \alpha 3\beta 2 > \alpha 3\beta 4$	[35]
RegIIA	<i>C. regius</i>	4/7	GCCSHPACNVNPHIC*	97	$\alpha 3\beta 2 > \alpha 3\beta 4 > \alpha 7$	[37]
Vc1.1	<i>C. victoriae</i>	4/7	GCCSDPRCNYDHPEIC*	4,200	$\alpha 9\alpha 10 > \alpha 6 / \alpha 3\beta 2\beta 3 > \alpha 6 / \alpha 3\beta 4 > \alpha 3\beta 4 > \alpha 3\beta 2$	[48]

* indicates a C-terminal amide.

Previous structure–activity relationship (SAR) studies with α -conotoxins have shown that the size of their Cys-loops may affect their pharmacological properties [49–51]. Most α -conotoxins have more notable effects on neuronal nAChRs than on muscle-type nAChRs when loop1 contains four amino acids. Some researchers have also demonstrated that the number of amino acids in loop2 affects the activity of α -conotoxins [52]. As shown in Table 4, $\alpha 4/4$ -conotoxin BuIA from *C. bullatus* showed insignificant subtype selectivity for nAChRs, although it exhibited high potency against $\alpha 3\beta 4$ nAChRs, with an IC₅₀ of 28 nM. Most natural $\alpha 4/7$ -conotoxins showed greater inhibitory activity against $\alpha 6 / \alpha 3\beta 4$ nAChRs than $\alpha 3\beta 4$ nAChRs, such as LvIA from *C. lividus*, PeIA from *C. pergrandis*, and Vc1.1 from *C. victoriae*. In contrast, natural $\alpha 4/6$ -conotoxins are more likely to interact with $\alpha 3\beta 4$ nAChRs. For example, AuIB identified from *C. aulicus* could specifically block $\alpha 3\beta 4$ nAChRs with an IC₅₀ of 750 nM, without obviously inhibiting other nAChRs. The inhibitory activity of $\alpha 4/6$ -conotoxin TxID against $\alpha 3\beta 4$ nAChRs was much higher than that of AuIB, and although it also inhibited $\alpha 6 / \alpha 3\beta 4$ nAChRs, it apparently had a stronger blocking effect on $\alpha 3\beta 4$ nAChRs. The results in this study showed that the 4/5-subfamily mutants had more severe inhibitory effects against $\alpha 3\beta 4$ and $\alpha 6 / \alpha 3\beta 4$ nAChRs than the 4/7-subfamily mutants, suggesting that the size of loop2 affects the potency of TxID. This may explain why the majority of natural α -conotoxins belonging to the 4/7-subfamily can block $\alpha 3\beta 4$ and $\alpha 6 / \alpha 3\beta 4$ nAChRs.

In this study, the loop2 size of α -conotoxin TxID was modified by insertion and truncation, after which the activities of all the mutants were assayed by electrophysiology. As the results showed, when Ser-9, Ala-10, and Met-11 were inserted with alanine or when the original amino acid was truncated, their activities were differentially reduced compared to the wild-type TxID. In previous studies, molecular simulations of TxID binding with $\alpha 6 / \alpha 3\beta 4$ nAChRs showed that Ser-9 of TxID formed a hydrogen bond with the $\beta 4$ subunit Lys-81 and was also spatially close to Glu-58, which explains the large loss of activity observed when we inserted Ser-9 [53]. The molecular model of TxID binding with $\alpha 3\beta 4$ nAChRs demonstrated that the deactivation of [+10A]TxID (which is the same as [+11A]TxID) and [Δ 11M]TxID was perhaps due to the contact between Met-11 from TxID and Cys-218 from the $\alpha 3$ subunit [53]. Previous studies concerning RegIIA have also shown that $\beta 4$ -K59 and $\beta 4$ -R113 formed hydrogen bonds with residues 9 and 11 of RegIIA, respectively, and that residue 10 formed non-conservative interactions with $\beta 4$ -I111 and

β 4-L119 [54]. Therefore, we hypothesized that changes to amino acids 9, 10, and 11 on loop2 of the TxID may affect its interactions with α 3 β 4 nAChRs.

As described by previous studies, there was a negatively charged Asp residue at position 14 in the α 4/6-conotoxin AuIB and a hydrophobic Ile at the corresponding position in the TxID, which may contribute to the different levels of potency and selectivity between AuIB and TxID [29,55]. In our research, the 4/7-subfamily mutant [+14A]TxID showed a greater decrease in activity compared to the other loop2 mutants of backward sites, with a 7.0-fold decrease in activity on α 3 β 4 and an 11-fold decrease in activity on α 6/ α 3 β 4. The NMR structure of TxID showed that one or both of the Pro residues underwent cis-trans isomerization, and the location of Pro-13 in loop2 attracted our attention [29]. Interestingly, the CD results of [+13A]TxID showed no significant changes in its secondary structure. However, a ten percent decrease in α -helices was observed in [Δ 13P]TxID, which was the most pronounced change among all the mutants. As the potency of [Δ 13P]TxID decreased in the α 3 β 4 and α 6/ α 3 β 4 nAChR activity by 22-fold and 44-fold, respectively, we hypothesized that Pro-13 slightly changed the structure of TxID and thus affected its activity.

Similar half maximal effective concentration (EC₅₀) values do not fully represent the same degree of receptor opening, so even though the EC₅₀ values of α 3 β 4 and α 6 β 4 nAChRs were similar, this study did not compare the IC₅₀ values between them [56]. This is very unfortunate for this study, but at the same time, provides a reference for future studies.

In summary, modifications to the loop2 size of α 4/6-conotoxin TxID resulting from inserting or truncating individual amino acids affected the activity of TxID targeting α 3 β 4 and α 6 β 4 nAChRs. This provides new insight for the further modification of α -conotoxin TxID and a unique perspective for studying the molecular mechanism of the interaction between α -conotoxins and the related receptors.

4. Materials and Methods

4.1. Materials and Animals

DH5 α competent cells and a plasmid extraction kit were purchased from Vazyme (Nanjing, China). Restriction enzymes, DNA markers, and DNA fragment purification kits were purchased from TaKaRa (Dalian, China). Reversed-phase C18 Vydac columns (5 μ m, 4.6 mm \times 250 mm; 10 μ m, 22 mm \times 250 mm) were purchased from Avantor (Radnor, PA, USA). Acetylcholine chloride, atropine, collagenase A, and bovine serum albumin (BSA) were purchased from Sigma (St. Louis, MO, USA). Acetonitrile (ACN, HPLC grade), cRNA mMACHINE in vitro transcription kits, and RNA MEGA Clear kits were purchased from Thermo Fisher Scientific (Pittsburgh, PA, USA). Trifluoroacetic acid (TFA) was purchased from Aladdin (Shanghai, China). All the other chemical reagents were of analytical grade.

cDNA clones encoding α 3 and β 4 subunits were kindly provided by S. Heinemann (Salk Institute, San Diego, CA, USA). The α 6/ α 3 chimera clone was generously provided by J. E. Garrett (Cognetix, Inc., Salt Lake City, UT, USA). Due to the poor expression of the natural α 6 subunit, the α 6/ α 3 subunit chimera was constructed in previous studies of α 6* nAChR expression in vitro, which includes the ECD of α 6 and the trans-membrane and intra-cellular domains of α 3 [35]. The β 4 subunit clone in the high expressing pGEMHE vector was generously provided by C. W. Luetje (University of Miami, Miami, FL, USA).

Female *Xenopus laevis* were obtained from Kunming Institute of Zoology (Kunming, China) and were maintained at 17 °C and fed twice a week for over 6 months before the experiments.

4.2. Peptide Synthesis

The linear peptides of TxID and its mutants were synthesized by GL Biochemistry (Shanghai, China) using the solid-phase peptide synthesis (SPPS) method. The first and third Cys residues of the peptides were protected in pairs with S-trityl (Trt), whereas

the second and fourth were protected with S-acetamidomethyl (Acm). The linear crude peptides were purified using RP-HPLC, and the final active peptides were obtained using a two-step oxidation protocol; all the procedures have been described previously [57,58]. The purification procedure of all linear, monocyclic, and bicyclic peptides was as follows: UV absorption wavelength at 214 nm and a linear gradient of 5–60% solvent B in 55 min at a flow rate of 15 mL/min, where solvent A was ddH₂O with 0.075% TFA and solvent B was 90% ACN and 10% ddH₂O with 0.05% TFA. An analytical RP-HPLC was utilized to confirm the purity (>95%) of all the mature peptides. The procedure was as follows: UV absorption wavelength at 214 nm and a linear gradient of 5–50% solvent B in 30 min at a flow rate of 1 mL/min. The molecular masses of the peptides were confirmed by ESI-MS.

4.3. Circular Dichroism (CD) Spectra

CD spectra were recorded at room temperature on a Jasco J-810 spectropolarimeter to determine the secondary structure of TxID and its mutants. Each sample was diluted with H₂O. The test conditions were as follows: a wavelength of 190–260 nm, a scanning rate of 100 nm/min, and a sample cell path length of 1 mm. Each trial had three replicates. The secondary structures of TxID and its mutants were calculated using the CDSSTR method.

4.4. cRNA Preparation and Injection

Plasmids containing cDNA clones of $\alpha 3$, $\alpha 6/\alpha 3$, and $\beta 4$ nAChR subunits were transformed into the DH5 α competent cell for storage and amplification. The cDNAs of the various subunits were linearized and purified with corresponding restriction enzymes, and their products were used as templates to obtain cRNAs by in vitro transcription with T3, T7, and SP6 mMACHINE transcription kits. The quality and concentration of cRNA were determined by electrophoresis and an ultraviolet spectrophotometer.

Oocytes were isolated from adult female *Xenopus laevis* and individual oocytes were obtained, as previously described [41]. The animal experiments were approved by the Ethics Committee of Guangxi University, and all the experimental procedures strictly complied with the guidelines for the care and use of laboratory animals. The oocytes were incubated in ND96 solution (96 mM NaCl, 2 mM KCl, 1.8 mM CaCl₂, 1 mM MgCl₂, and 5 mM HEPES, pH 7.1–7.5) with antibiotics (10 mg/L penicillin, 10 mg/L streptomycin, and 100 mg/L gentamicin) at 17 °C and at 35% humidity. Glass needles for microinjection were pulled using a P-1000 needle puller (Sutter Instrument Corp., Novato, CA, USA). The cRNAs of different subunits of nAChRs were mixed in equimolar ratios, which were then injected into the oocytes within 24 h of oocyte harvest, ensuring that at least 10 ng of each subunit was injected for each individual oocyte.

4.5. Voltage Clamp Recording

The membrane currents of injected *Xenopus* oocytes were recorded 2–3 days after injection using a two-electrode voltage clamp amplifier (OC-725D, WARNER Instrument, Holliston, MA, USA) and a digital-to-analog converter (Axon 1550B, Molecular Devices, Sunnyvale, CA, USA). The recording electrodes with suitable tips were made from borosilicate glass and had a resistance of 0.5–2 M Ω when filled with 3 M KCl. The oocytes were placed in a cylindrical chamber with a volume of approximately 50 μ L and were clamped at a holding potential of –70 mV. During the data recording period, the oocytes were perfused at a flow rate of 2–4 mL/min with ND96 buffer containing 0.1 mg/mL BSA and 1 μ M atropine gravitationally, whereas a 2 s pulse of 100 μ M ACh was applied per minute to induce the inward current. The oocytes were incubated with ND96 and current values were obtained after ACh stimulation, which were taken as the control responses. The average peak amplitude of the three control responses was used as a baseline. When the TxID and its mutants were incubated, 5 μ L of ND96 buffer was removed and replaced with different concentrations of peptides and the currents were recorded after 5 min of incubation. The ratio of ACh-induced current to baseline current after 5 min of incubation with different concentrations of TxID and its mutants allowed us to identify their blocking effects.

4.6. Statistical Analysis of Data

GraphPad Prism 7.0 (GraphPad Software, San Diego, CA, USA) was used to fit the data and draw the graphs. The dose–response curves were fitted using non-linear regression according to the following equation: $\text{Response}\% = 100/[1 + ([\text{toxin}]/\text{IC}_{50})^{\text{nH}}]$, where nH represents the Hill coefficient and IC_{50} represents the concentration of the antagonist that produces half-maximal inhibition. All the data points on the dose-response curves were fitted using the mean \pm SEM, and each data point was replicated in at least six oocytes, which were obtained from different individual *Xenopus laevis* to ensure the reproducibility and accuracy of the results.

Supplementary Materials: The following supporting information can be downloaded at: <https://www.mdpi.com/article/10.3390/md21050286/s1>, additional figures illustrating the RP-HPLC and ESI-MS analysis of TxID and its mutants (Figures S1 and S2).

Author Contributions: J.Y. and S.L. conceived and designed the experiments; J.D., P.Z. and J.X. performed the experiments; J.D. and T.X. analyzed the data; J.D., X.Z., J.Y., D.Z. and S.L. wrote and revised the manuscript. All authors have read and agreed to the published version of the manuscript.

Funding: This research was funded in part by the Guangxi Natural Science Foundation (No. 2022GXNSFBA035662), the Guangxi Science and Technology Base and Talents Fund (GUIKE AD22035948), the Major Intergovernmental Joint Research Project of the National Key R&D Program of China (2022YFE0132700), the 111 Project (D20010), and the National Natural Science Foundation of China (Nos. 82104059, 81872794, 41966003).

Institutional Review Board Statement: Not applicable.

Informed Consent Statement: Not applicable.

Data Availability Statement: The data presented in this study are available in the article.

Conflicts of Interest: The authors declare that they have no known competing financial interests or personal relationships that could have appeared to influence the work reported in this paper.

Abbreviations Used

ACh, acetylcholine chloride; ACN, acetonitrile; Acm, S-acetamidomethyl; BSA, bovine serum albumin; CI, confidence interval; ESI-MS, electrospray ionization mass spectroscopy; IC_{50} , half maximal inhibitory concentration; $\text{K}_3[\text{Fe}(\text{CN})_6]$, potassium ferricyanide; MW, molecular mass; nAChRs, nicotinic acetylcholine receptors; RP-HPLC, reversed-phase high-performance liquid chromatography; SPPS, solid-phase peptide synthesis; Trt, S-trityl; TFA, trifluoroacetic acid.

References

1. Corradi, J.; Bouzat, C. Understanding the Bases of Function and Modulation of $\alpha 7$ Nicotinic Receptors: Implications for Drug Discovery. *Mol. Pharmacol.* **2016**, *90*, 288–299. [[CrossRef](#)] [[PubMed](#)]
2. Olivera, B.M.; Quik, M.; Vincler, M.; McIntosh, J.M. Subtype-selective conopeptides targeted to nicotinic receptors: Concerted discovery and biomedical applications. *Channels* **2008**, *2*, 143–152. [[CrossRef](#)] [[PubMed](#)]
3. Gharpure, A.; Noviello, C.M.; Hibbs, R.E. Progress in nicotinic receptor structural biology. *Neuropharmacology* **2020**, *171*, 108086. [[CrossRef](#)] [[PubMed](#)]
4. Ho, T.N.T.; Abraham, N.; Lewis, R.J. Structure-Function of Neuronal Nicotinic Acetylcholine Receptor Inhibitors Derived From Natural Toxins. *Front. Neurosci.* **2020**, *14*, 609005. [[CrossRef](#)] [[PubMed](#)]
5. Smith, N.J.; Hone, A.J.; Memon, T.; Bossi, S.; Smith, T.E.; McIntosh, J.M.; Olivera, B.M.; Teichert, R.W. Comparative functional expression of nAChR subtypes in rodent DRG neurons. *Front. Cell Neurosci.* **2013**, *7*, 225. [[CrossRef](#)]
6. Liu, Y.; Qian, J.; Sun, Z.; Zhangsun, D.; Luo, S. Cervical Cancer Correlates with the Differential Expression of Nicotinic Acetylcholine Receptors and Reveals Therapeutic Targets. *Mar. Drugs.* **2019**, *17*, 256. [[CrossRef](#)]
7. Hone, A.J.; McIntosh, J.M.; Azam, L.; Lindstrom, J.; Lucero, L.; Whiteaker, P.; Passas, J.; Blazquez, J.; Albillos, A. α -Conotoxins Identify the $\alpha 3\beta 4^*$ Subtype as the Predominant Nicotinic Acetylcholine Receptor Expressed in Human Adrenal Chromaffin Cells. *Mol. Pharmacol.* **2015**, *88*, 881–893. [[CrossRef](#)]
8. Rivera-Perez, L.M.; Kwapiszewski, J.T.; Roberts, M.T. $\alpha(3)\beta(4)^*$ Nicotinic Acetylcholine Receptors Strongly Modulate the Excitability of VIP Neurons in the Mouse Inferior Colliculus. *Front. Neural. Circuits* **2021**, *15*, 709387. [[CrossRef](#)]

9. Grady, S.R.; Moretti, M.; Zoli, M.; Marks, M.J.; Zanardi, A.; Pucci, L.; Clementi, F.; Gotti, C. Rodent habenulo-interpeduncular pathway expresses a large variety of uncommon nAChR subtypes, but only the $\alpha 3\beta 4^*$ and $\alpha 3\beta 3\beta 4^*$ subtypes mediate acetylcholine release. *J. Neurosci.* **2009**, *29*, 2272–2282. [[CrossRef](#)]
10. Cao, Y.J.; Surowy, C.S.; Puttfarcken, P.S. Nicotinic acetylcholine receptor-mediated [3H]dopamine release from hippocampus. *J. Pharmacol. Exp. Ther.* **2005**, *312*, 1298–1304. [[CrossRef](#)]
11. Yuan, M.; Malagon, A.M.; Yasuda, D.; Belluzzi, J.D.; Leslie, F.M.; Zaveri, N.T. The $\alpha 3\beta 4$ nAChR partial agonist AT-1001 attenuates stress-induced reinstatement of nicotine seeking in a rat model of relapse and induces minimal withdrawal in dependent rats. *Behav. Brain Res.* **2017**, *333*, 251–257. [[CrossRef](#)] [[PubMed](#)]
12. Stoker, A.K.; Markou, A. Unraveling the neurobiology of nicotine dependence using genetically engineered mice. *Curr. Opin. Neurobiol.* **2013**, *23*, 493–499. [[CrossRef](#)] [[PubMed](#)]
13. Wills, L.; Ables, J.L.; Braunscheidel, K.M.; Caligiuri, S.P.B.; Elayouby, K.S.; Fillinger, C.; Ishikawa, M.; Moen, J.K.; Kenny, P.J. Neurobiological Mechanisms of Nicotine Reward and Aversion. *Pharmacol. Rev.* **2022**, *74*, 271–310. [[CrossRef](#)]
14. Letchworth, S.R.; Whiteaker, P. Progress and challenges in the study of $\alpha 6$ -containing nicotinic acetylcholine receptors. *Biochem. Pharmacol.* **2011**, *82*, 862–872. [[CrossRef](#)] [[PubMed](#)]
15. Azam, L.; McIntosh, J.M. Characterization of nicotinic acetylcholine receptors that modulate nicotine-evoked [3H]norepinephrine release from mouse hippocampal synaptosomes. *Mol. Pharmacol.* **2006**, *70*, 967–976. [[CrossRef](#)] [[PubMed](#)]
16. Quik, M.; Perez, X.A.; Grady, S.R. Role of $\alpha 6$ nicotinic receptors in CNS dopaminergic function: Relevance to addiction and neurological disorders. *Biochem. Pharmacol.* **2011**, *82*, 873–882. [[CrossRef](#)]
17. Hone, A.J.; Meyer, E.L.; McIntyre, M.; McIntosh, J.M. Nicotinic acetylcholine receptors in dorsal root ganglion neurons include the $\alpha 6\beta 4$ subtype. *FASEB J.* **2012**, *26*, 917–926. [[CrossRef](#)]
18. Wieskopf, J.S.; Mathur, J.; Limapichat, W.; Post, M.R.; Al-Qazzaz, M.; Sorge, R.E.; Martin, L.J.; Zaykin, D.V.; Smith, S.B.; Freitas, K.; et al. The nicotinic $\alpha 6$ subunit gene determines variability in chronic pain sensitivity via cross-inhibition of P2X2/3 receptors. *Sci. Transl. Med.* **2015**, *7*, 287ra72. [[CrossRef](#)]
19. Lebbe, E.K.; Peigneur, S.; Wijesekara, I.; Tytgat, J. Conotoxins targeting nicotinic acetylcholine receptors: An overview. *Mar. Drugs* **2014**, *12*, 2970–3004. [[CrossRef](#)]
20. Sanchez-Campos, N.; Bernaldez-Sarabia, J.; Licea-Navarro, A.F. Conotoxin Patenting Trends in Academia and Industry. *Mar. Drugs* **2022**, *20*, 531. [[CrossRef](#)]
21. Akondi, K.B.; Muttenthaler, M.; Dutertre, S.; Kaas, Q.; Craik, D.J.; Lewis, R.J.; Alewood, P.F. Discovery, synthesis, and structure-activity relationships of conotoxins. *Chem. Rev.* **2014**, *114*, 5815–5847. [[CrossRef](#)] [[PubMed](#)]
22. Margiotta, F.; Micheli, L.; Ciampi, C.; Ghelardini, C.; McIntosh, J.M.; Di Cesare Mannelli, L. Conus regius-Derived Conotoxins: Novel Therapeutic Opportunities from a Marine Organism. *Mar. Drugs* **2022**, *20*, 773. [[CrossRef](#)]
23. Nicke, A.; Wonnacott, S.; Lewis, R.J. Alpha-conotoxins as tools for the elucidation of structure and function of neuronal nicotinic acetylcholine receptor subtypes. *Eur. J. Biochem.* **2004**, *271*, 2305–2319. [[CrossRef](#)]
24. Azam, L.; McIntosh, J.M. Alpha-conotoxins as pharmacological probes of nicotinic acetylcholine receptors. *Acta Pharmacol. Sin.* **2009**, *30*, 771–783. [[CrossRef](#)]
25. Daly, J.W. Nicotinic agonists, antagonists, and modulators from natural sources. *Cell Mol. Neurobiol.* **2005**, *25*, 513–552. [[CrossRef](#)] [[PubMed](#)]
26. Kaas, Q.; Westermann, J.C.; Craik, D.J. Conopeptide characterization and classifications: An analysis using ConoServer. *Toxicon* **2010**, *55*, 1491–1509. [[CrossRef](#)]
27. Ma, Q.; Tae, H.S.; Wu, G.; Jiang, T.; Yu, R. Exploring the Relationship between Nicotinic Acetylcholine Receptor Ligand Size, Efficiency, Efficacy, and C-Loop Opening. *J. Chem. Inf. Model* **2017**, *57*, 1947–1956. [[CrossRef](#)]
28. Jin, A.H.; Muttenthaler, M.; Dutertre, S.; Himaya, S.W.A.; Kaas, Q.; Craik, D.J.; Lewis, R.J.; Alewood, P.F. Conotoxins: Chemistry and Biology. *Chem. Rev.* **2019**, *119*, 11510–11549. [[CrossRef](#)] [[PubMed](#)]
29. Luo, S.; Zhangsun, D.; Zhu, X.; Wu, Y.; Hu, Y.; Christensen, S.; Harvey, P.J.; Akcan, M.; Craik, D.J.; McIntosh, J.M. Characterization of a novel alpha-conotoxin TxID from Conus textile that potently blocks rat $\alpha 3\beta 4$ nicotinic acetylcholine receptors. *J. Med. Chem.* **2013**, *56*, 9655–9663. [[CrossRef](#)]
30. Qian, J.; Liu, Y.Q.; Sun, Z.H.; Zhangsun, D.T.; Luo, S.L. Identification of nicotinic acetylcholine receptor subunits in different lung cancer cell lines and the inhibitory effect of alpha-conotoxin TxID on lung cancer cell growth. *Eur. J. Pharmacol.* **2019**, *865*, 172674. [[CrossRef](#)] [[PubMed](#)]
31. Gehrman, J.; Alewood, P.F.; Craik, D.J. Structure determination of the three disulfide bond isomers of α -conotoxin GI: A model for the role of disulfide bonds in structural stability. Edited by P. E. Wright. *J. Mol. Biol.* **1998**, *278*, 401–415. [[CrossRef](#)]
32. Wilhelm, P.; Luna-Ramirez, K.; Chin, Y.K.Y.; Dekan, Z.; Abraham, N.; Tae, H.-S.; Chow, C.Y.; Eagles, D.A.; King, G.F.; Lewis, R.J.; et al. Cysteine-Rich α -Conotoxin SII Displays Novel Interactions at the Muscle Nicotinic Acetylcholine Receptor. *ACS Chem. Neurosci.* **2022**, *13*, 1245–1250. [[CrossRef](#)]
33. Guo, H.; Deng, B.; Zhao, L.; Gao, Y.; Zhang, X.; Yang, C.; Zou, B.; Chen, H.; Sun, M.; Wang, L.; et al. Programmed Aptamer Screening, Characterization, and Rapid Detection for alpha-Conotoxin MI. *Toxins* **2022**, *14*, 706. [[CrossRef](#)] [[PubMed](#)]
34. Chi, S.W.; Kim, D.H.; Olivera, B.M.; McIntosh, J.M.; Han, K.H. Solution conformation of a neuronal nicotinic acetylcholine receptor antagonist alpha-conotoxin OmIA that discriminates $\alpha 3$ vs. $\alpha 6$ nAChR subtypes. *Biochem. Biophys Res. Commun.* **2006**, *345*, 248–254. [[CrossRef](#)] [[PubMed](#)]

35. Dowell, C.; Olivera, B.M.; Garrett, J.E.; Staheli, S.T.; Watkins, M.; Kuryatov, A.; Yoshikami, D.; Lindstrom, J.M.; McIntosh, J.M. α -Conotoxin PIA Is Selective for $\alpha 6$ Subunit-Containing Nicotinic Acetylcholine Receptors. *J. Neurosci.* **2003**, *23*, 8445–8452. [[CrossRef](#)] [[PubMed](#)]
36. Spira, M.E.; Hasson, A.; Fainzilber, M.; Gordon, D.; Zlotkin, E. Chemical and electrophysiological characterization of new peptide neurotoxins from the venom of the molluscivorous snail *Conus textile neovicarius*: A review. *Isr. J. Med. Sci.* **1993**, *29*, 530–543.
37. Franco, A.; Kompella, S.N.; Akondi, K.B.; Melaun, C.; Daly, N.L.; Luetje, C.W.; Alewood, P.F.; Craik, D.J.; Adams, D.J.; Mari, F. RegIIA: An $\alpha 4/7$ -conotoxin from the venom of *Conus regius* that potently blocks $\alpha 3\beta 4$ nAChRs. *Biochem. Pharmacol.* **2012**, *83*, 419–426. [[CrossRef](#)]
38. McIntosh, J.M.; Plazas, P.V.; Watkins, M.; Gomez-Casati, M.E.; Olivera, B.M.; Elgoyhen, A.B. A novel alpha-conotoxin, PeIA, cloned from *Conus pergrandis*, discriminates between rat $\alpha 9\alpha 10$ and $\alpha 7$ nicotinic cholinergic receptors. *J. Biol. Chem.* **2005**, *280*, 30107–30112. [[CrossRef](#)]
39. Inserra, M.C.; Kompella, S.N.; Vetter, I.; Brust, A.; Daly, N.L.; Cuny, H.; Craik, D.J.; Alewood, P.F.; Adams, D.J.; Lewis, R.J. Isolation and characterization of alpha-conotoxin LsIA with potent activity at nicotinic acetylcholine receptors. *Biochem. Pharmacol.* **2013**, *86*, 791–799. [[CrossRef](#)]
40. Kompella, S.N.; Hung, A.; Clark, R.J.; Mari, F.; Adams, D.J. Alanine scan of alpha-conotoxin RegIIA reveals a selective $\alpha 3\beta 4$ nicotinic acetylcholine receptor antagonist. *J. Biol. Chem.* **2015**, *290*, 1039–1048. [[CrossRef](#)]
41. Hogg, R.C.; Hopping, G.; Alewood, P.F.; Adams, D.J.; Bertrand, D. Alpha-conotoxins PnIA and [A10L]PnIA stabilize different states of the $\alpha 7$ -L247T nicotinic acetylcholine receptor. *J. Biol. Chem.* **2003**, *278*, 26908–26914. [[CrossRef](#)] [[PubMed](#)]
42. Luo, S.; Kulak, J.M.; Cartier, G.E.; Jacobsen, R.B.; Yoshikami, D.; Olivera, B.M.; McIntosh, J.M. α -Conotoxin AuIB Selectively Blocks $\alpha 3\beta 4$ Nicotinic Acetylcholine Receptors and Nicotine-Evoked Norepinephrine Release. *J. Neurosci.* **1998**, *18*, 8571–8579. [[CrossRef](#)]
43. van Hout, M.; Valdes, A.; Christensen, S.B.; Tran, P.T.; Watkins, M.; Gajewiak, J.; Jensen, A.A.; Olivera, B.M.; McIntosh, J.M. α -Conotoxin VnIB from *Conus ventricosus* is a potent and selective antagonist of $\alpha 6\beta 4^*$ nicotinic acetylcholine receptors. *Neuropharmacology* **2019**, *157*, 107691. [[CrossRef](#)] [[PubMed](#)]
44. Azam, L.; Dowell, C.; Watkins, M.; Stitzel, J.A.; Olivera, B.M.; McIntosh, J.M. Alpha-conotoxin BuIA, a novel peptide from *Conus bullatus*, distinguishes among neuronal nicotinic acetylcholine receptors. *J. Biol. Chem.* **2005**, *280*, 80–87. [[CrossRef](#)] [[PubMed](#)]
45. Azam, L.; Maskos, U.; Changeux, J.P.; Dowell, C.D.; Christensen, S.; De Biasi, M.; McIntosh, J.M. alpha-Conotoxin BuIA[T5A;P6O]: A novel ligand that discriminates between $\alpha 6\beta 4$ and $\alpha 6\beta 2$ nicotinic acetylcholine receptors and blocks nicotine-stimulated norepinephrine release. *FASEB J.* **2010**, *24*, 5113–5123. [[CrossRef](#)]
46. Luo, S.; Zhangsun, D.; Schroeder, C.I.; Zhu, X.; Hu, Y.; Wu, Y.; Weltzin, M.M.; Eberhard, S.; Kaas, Q.; Craik, D.J.; et al. A novel $\alpha 4/7$ -conotoxin LvIA from *Conus lividus* that selectively blocks $\alpha 3\beta 2$ vs. $\alpha 6/\alpha 3\beta 2\beta 3$ nicotinic acetylcholine receptors. *FASEB J.* **2014**, *28*, 1842–1853. [[CrossRef](#)]
47. Hone, A.J.; Ruiz, M.; Scadden, M.; Christensen, S.; Gajewiak, J.; Azam, L.; McIntosh, J.M. Positional scanning mutagenesis of alpha-conotoxin PeIA identifies critical residues that confer potency and selectivity for $\alpha 6/\alpha 3\beta 2\beta 3$ and $\alpha 3\beta 2$ nicotinic acetylcholine receptors. *J. Biol. Chem.* **2013**, *288*, 25428–25439. [[CrossRef](#)]
48. Vincler, M.; Wittenauer, S.; Parker, R.; Ellison, M.; Olivera, B.M.; McIntosh, J.M. Molecular mechanism for analgesia involving specific antagonism of $\alpha 9\alpha 10$ nicotinic acetylcholine receptors. *Proc. Natl. Acad. Sci. USA* **2006**, *103*, 17880–17884. [[CrossRef](#)]
49. Turner, M.; Eidemiller, S.; Martin, B.; Narver, A.; Marshall, J.; Zemp, L.; Cornell, K.A.; McIntosh, J.M.; McDougal, O.M. Structural basis for alpha-conotoxin potency and selectivity. *Bioorg. Med. Chem.* **2009**, *17*, 5894–5899. [[CrossRef](#)] [[PubMed](#)]
50. Loughnan, M.L.; Alewood, P.F. Physico-chemical characterization and synthesis of neuronally active alpha-conotoxins. *Eur. J. Biochem.* **2004**, *271*, 2294–2304. [[CrossRef](#)]
51. Craig, A.G.; Bandyopadhyay, P.; Olivera, B.M. Post-translationally modified neuropeptides from *Conus* venoms. *Eur. J. Biochem.* **1999**, *264*, 271–275. [[CrossRef](#)]
52. Giribaldi, J.; Dutertre, S. alpha-Conotoxins to explore the molecular, physiological and pathophysiological functions of neuronal nicotinic acetylcholine receptors. *Neurosci. Lett.* **2018**, *679*, 24–34. [[CrossRef](#)] [[PubMed](#)]
53. Wu, Y.; Zhangsun, D.; Zhu, X.; Kaas, Q.; Zhangsun, M.; Harvey, P.J.; Craik, D.J.; McIntosh, J.M.; Luo, S. alpha-Conotoxin [S9A]TxID Potently Discriminates between $\alpha 3\beta 4$ and $\alpha 6/\alpha 3\beta 4$ Nicotinic Acetylcholine Receptors. *J. Med. Chem.* **2017**, *60*, 5826–5833. [[CrossRef](#)] [[PubMed](#)]
54. Xu, Q.; Tae, H.S.; Wang, Z.; Jiang, T.; Adams, D.J.; Yu, R. Rational Design of alpha-Conotoxin RegIIA Analogues Selectively Inhibiting the Human $\alpha 3\beta 2$ Nicotinic Acetylcholine Receptor through Computational Scanning. *ACS Chem. Neurosci.* **2020**, *11*, 2804–2811. [[CrossRef](#)] [[PubMed](#)]
55. Lee, B.H.; Hwang, S.H.; Choi, S.H.; Shin, T.J.; Kang, J.; Lee, S.M.; Nah, S.Y. Quercetin Inhibits $\alpha 3\beta 4$ Nicotinic Acetylcholine Receptor-Mediated Ion Currents Expressed in *Xenopus* Oocytes. *Korean J. Physiol. Pharmacol.* **2011**, *15*, 17–22. [[CrossRef](#)] [[PubMed](#)]
56. Germann, A.L.; Pierce, S.R.; Evers, A.S.; Steinbach, J.H.; Akk, G. Perspective on the Relationship between GABAA Receptor Activity and the Apparent Potency of an Inhibitor. *Curr. Neuropharmacol.* **2022**, *20*, 90–93. [[CrossRef](#)]

57. Fuller, E.; Green, B.R.; Catlin, P.; Buczek, O.; Nielsen, J.S.; Olivera, B.M.; Bulaj, G. Oxidative folding of conotoxins sharing an identical disulfide bridging framework. *FEBS J.* **2005**, *272*, 1727–1738. [[CrossRef](#)]
58. Steiner, A.M.; Bulaj, G. Optimization of oxidative folding methods for cysteine-rich peptides: A study of conotoxins containing three disulfide bridges. *J. Pept. Sci.* **2011**, *17*, 1–7. [[CrossRef](#)]

Disclaimer/Publisher’s Note: The statements, opinions and data contained in all publications are solely those of the individual author(s) and contributor(s) and not of MDPI and/or the editor(s). MDPI and/or the editor(s) disclaim responsibility for any injury to people or property resulting from any ideas, methods, instructions or products referred to in the content.